Structure and composition of first biosourced Mn-rich catalysts with a unique vegetal footprint

Claire Garel, Emiliano Fonda, Alain Michalowicz, S. Diliberto, Clotilde Boulanger, Eddy Petit, Yves-Marie Legrand, Cyril Poullain, Claude Grison

Structure and composition of first biosourced Mn-rich catalysts with a unique vegetal footprint

C. Garel [a], E. Fonda [b], A. Michalowicz [c], S. Diliberto [d], C. Boulanger [d], E. Petit [e], Y.M. Legrand [e], C. Poullain [a], C. Grison [a, *]

[a] Laboratoire de Chimie Bio-inspirée et d'Innovations Ecologiques, UMR 5021, Centre National de la Recherche Scientifique, Université de Montpellier, 34790 Grabels, France
[b] Synchrotron SOLEIL, 91190 Saint Aubin, France
[c] Institute of Chemistry and Materials Paris East, UMR 7182, Centre National de la Recherche Scientifique, University Paris East Creteil, 94320 Thiais, France
[d] Institut Jean Lamour, UMR 7198, Centre National de la Recherche Scientifique, Université de Lorraine, 57078 Metz, France
[e] Institut Européen des Membranes (IEM), UMR 5635, ENSCM, Centre National de la Recherche Scientifique, Université de Montpellier, 34095 Montpellier, France

ARTICLE INFO

Keywords:
Ecological rehabilitation
Bio-based materials
Ecocatalysts
Structural study

ABSTRACT

Ecological rehabilitation of degraded mining sites is necessary and possible by reintroducing pioneer manganese-accumulating plants. From the Mn-enriched biomass, our group has developed a process to recycle plant-derived metallic elements into innovative polymetallic catalysts, called Eco-Mn ecocatalysts. These first biosourced Mn-rich catalysts have demonstrated competitive catalytic activity in green organic synthesis. To expand the use of these catalysts in organic chemistry, their catalytic activity has to be correlated with their structure and properties. Thus, we put forward for the first time an extensive structural study of Eco-Mn catalysts, including composition analysis, crystalline structure analysis, and chemical environment around active catalytic center (manganese and iron) analysis. Density Functional Theory (DFT) calculations support our conclusions. Finally, this study highlights the peculiar vegetal footprint of Eco-Mn catalysts.

1. Introduction

Inescapable and intensive exploitation of mineral resources generates serious environmental damage by the dissemination of "trace metallic elements" throughout the environment [1]. New Caledonia provides an illustrative example of this situation as it is widely known as a biodiversity 'hot spot' [2] that is jeopardized by intensive mining activities. This archipelago holds a large part of the world's nickel reserves [3], with 25 mines that have been exploited since 1873 [4]. Reaching exploitable nickel ores requires removing the fertile upper horizons of the soil, producing open-cast mines [4,5]. This creates serious environmental problems: stripped soils are exposed to rainfall, leading to erosion that threatens terrestrial ecosystems and estuaries [4,6]. Moreover, the scarcity of organic matter in these bare soils inhibits spontaneous reestablishment of vegetation cover [5,7].

Thus, ecological rehabilitation of mining sites by active reintroduction of the vegetation cover is necessary. Fortunately, the endemic biodiversity of New Caledonia includes plants possessing an impressive adaptability to metal (manganese and nickel) concentrations in soils. Some endemic species have the ability to accumulate or hyperaccumulate nickel or manganese from the soil into their aerial parts [8–10]. These plants are assets for the ecological rehabilitation of mining sites, especially pioneer plants [5,7,11], which are the most resistant to climatic and edaphic conditions and are the first to be reintroduced.

Our group has demonstrated that it is possible to rehabilitate New Caledonian mining sites by reintroducing pioneer Mn- and Ni-accumulating plants. Manganese accumulators in the genus *Grevillea* (Proteaceae) are mainly used to restore mining sites across both provinces of New Caledonia, as they represent 58% of plant species used by our team [12,13].

In order to provide scientific and economic outlets for such ecological programs, we have shown that Mn-rich biomass can be turned into efficient catalysts through an innovative concept: ecocatalysis [7, 12–17]. Based on the ability of *Grevillea* species to

* Corresponding author.
E-mail address: claude.grison@cnrs.fr (C. Grison).

https://doi.org/10.1016/j.mtsust.2019.100020

concentrate manganese in their shoots, we developed an innovative concept to transform plant-derived manganese into 'green' catalysts, also known as Eco-Mn ecocatalysts. Eco-Mn ecocatalysts are the first biosourced manganese-rich catalysts.

Eco-Mn revealed an original polymetallic composition resulting in marked Brønsted and Lewis acidities and displayed superior catalytic performances to conventional Mn catalysts [7,18]. For example, Eco-Mn was successfully used in the aminoreduction ketones. This result constitutes the first example of reduction, which has been promoted by a Mn catalyst [19]. Besides the extension of such Mn-catalyzed reductions, we described oxidative cleavages of 1,2-diols into aldehyde or ketones using Eco-Mn and Eco-Mn_{ox} as catalysts [20]. Eco-Mn catalysts have also been demonstrated to serve as green catalysts for valuable epoxidation reactions. In order to understand their catalytic activity, properties of Eco-Mn were compared to those of commercial salts. This comparison highlighted the peculiar composition and structure of Eco-Mn catalysts [21].

Eco-Mn catalysts have recently attracted broad research interest as they combine the merits of both green catalysts and ecological approach. Rational design and preparation of Eco-Mn are of immense significance but have so far been plagued by the lack of a definitive correlation between structure and catalytic properties. The unprecise nature of the catalyst precludes accurate mechanistic studies. Here, we report an extensive structural study of a series of Eco-Mn, using inductively coupled plasma mass spectrometry (ICP-MS), X-ray diffraction (XRD), X-ray absorption near-edge structure, and extended X-ray absorption fine structure analyses, which are completed by DFT calculations. Finally, a prominent aim of this work was to illustrate the vegetal footprint of Eco-Mn.

2. Materials and methods

2.1. General part

The blender used to crush the biomass is a Waring Blender from Dutscher. An oven KK100/12 ThermConcept was used for all the thermal treatments. The temperature program generally used, named P1, is as follow: 25—550 °C in 1 h and 4 h at 550 °C.

Commercial salts used to synthesize manganese malate trihydrate and synthetic catalysts, and commercial salts used as references in X-ray absorption spectroscopy (XAS) studies, come from Sigma Aldrich, Alfa Aesar, Merck Millipore, or Carlo Erba.

2.2. Eco-Mn synthesis

Eco-Mn catalysts were prepared from harvested leaves of New Caledonian manganese-accumulating plants (*Grevillea exul* ssp. *exul*, *Grevillea exul* ssp. *rubiginosa*, *Grevillea gillivrayi*, *Grevillea meisneri*, and *Garcinia amplexicaulis*). Plants' leaves were harvested by hand in New Caledonia on the different mining sites, which are currently rehabilitated by our team. Harvests are made respecting legal authorizations.

Harvested biomass is sent to our laboratory, air dried at ambient temperature, and ground. The obtained powder is thermally treated in an oven under air flow with the temperature program P1. Obtained ashes are carefully introduced at ambient temperature in hydrochloric acid solutions more or less concentrated:

- In case of Eco-Mn_1, Eco-Mn_2, Eco-Mn_3, Eco-Mn_4, and Eco-Mn_5, 1 g of ashes was introduced in 10 mL of 12 M HCl.
- In case of Eco-Mn_6, Eco-Mn_7, and Eco-Mn_8, 1 g of ashes was introduced in 30 mL of 4 M HCl.
- In case of Eco-Mn_9 and Eco-Mn_{10}, 1 g of ashes was introduced in 120 mL of 1 M HCl.

The obtained mixture was stirred for 4 h at 80 °C and overnight at ambient temperature.

The reaction mixture was then filtered on a pad of celite previously washed with a 12 M HCl solution. In case of Eco-Mn_6, Eco-Mn_7, Eco-Mn_8, Eco-Mn_9, and Eco-Mn_{10}, the pad of Celite was washed second time with 4 M (resp. 1 M) HCl. Then, the filtered solid on the Celite was washed four times with 15 mL of a 12 M (resp. 4 M, and 1 M) HCl solution.

The amber solution recovered after filtration was concentrated under vacuum, with the following program: 1 h 30 min at 60 mbar and 60 °C, then 1 h 30 min at 30 mbar and 60 °C, and 1 h 30 min at 30 mbar and 80 °C. This yields to an ecocatalyst Eco-Mn as pale yellow powder. Eco-Mn was stored in an oven at 100 °C during about four days, then under vacuum in a desiccator.

2.3. Manganese malate trihydrate ($MnC_4H_4O_5.3H_2O$) synthesis

Manganese malate trihydrate synthesis is based on the protocol described by Lenstra and Dillen [22]. To a beaker, 17.50 g of malic acid (0.131 mol, 1.5 eq.) and 100 mL of deionised water were added. Ten grams of anhydrous $MnCO_3$ (0.087 mol, 1 eq.) was then added. The brown mixture was stirred for 2 h and left overnight at ambient temperature. A pale pink solid is collected at the bottom of the beaker, washed with 10 mL of deionised water, and stored under vacuum in a desiccator. Synthesis of $MnC_4H_4O_5.3H_2O$ has been checked by IR spectroscopy and by measuring Mn weight percentage in the obtained product by ICP-MS analysis.

2.4. Synthetic catalysts (Syn-Mn_1, Syn-Mn_2, Syn-Mn_2'/$MnMg_2Cl_6.12H_2O$) synthesis

2.4.1. Syn-Mn_1

955.4 mg of $MnCl_2.4H_2O$ (4.83 mmol), 429.5 mg of anhydrous $CaCl_2$ (3.87 mmol), 621.7 mg of anhydrous $MgCl_2$ (6.53 mmol), 202.3 mg of NaCl (3.46 mmol), 553.7 mg of KCl (7.43 mmol), 156.8 mg of $FeCl_3.6H_2O$ (0.58 mmol), 29.2 mg of $NiCl_2.6H_2O$ (0.12 mmol), and 55.8 mg of anhydrous $AlCl_3$ (0.42 mmol) were introduced in a round bottom flask. The mixture was stirred under vacuum (about 2.10^{-1} mbar) for several hours, in order to get a homogeneous and fine powder. This catalyst Syn-Mn_1 was stored under vacuum in a desiccator.

2.4.2. Syn-Mn_2

1163.6 mg of $MnC_4H_4O_5.3H_2O$ (4.83 mmol), 565.4 mg of $CaC_2O_4.2H_2O$ (3.87 mmol), 807.4 mg of $Mg_3(PO_4)_2.xH_2O$ (x chosen equal to 6) (2.18 mmol), 202.3 mg of NaCl (3.46 mmol), 553.7 mg of KCl (7.43 mmol), 108.4 mg of $FePO_4.2H_2O$ (0.58 mmol), 32.2 mg of $NiSO_4.6H_2O$ (0.12 mmol), and 70.4 mg of $Al_2C_6O_{12}.xH_2O$ (x chosen equal to 1) (0.21 mmol) were added to a round bottom flask. The mixture was stirred under vacuum (about 2.10^{-1} mbar) during several hours in order to get a fine and homogeneous powder. This powder was thermally treated in an oven under air flow, following the temperature programme P1. Obtained ashes were chemically activated following exactly the same general procedure as the one used to produce Eco-Mn_1.

2.4.3. Syn-Mn_2'/$MnMg_2Cl_6.12H_2O$

Syn-Mn_2' is produced by following exactly the same experimental procedure as for Syn-Mn_2 but by introducing 2422.1 mg of $Mg_3(PO_4)_2.xH_2O$ (6.53 mmol) instead of 807.4 mg and 907.6 mg of $MnC_4H_4O_5.3H_2O$ (3.76 mmol) instead of 1163.6 mg.

2.5. Control catalyst, transmission electronic microscopy (Tem)-Mn, synthesis

Grevillea rosa ssp. *jenkinsii* was bought in a garden center in Montpellier. Leaves were harvested by hand and air dried at 60 °C in an oven during 24h00. Dried leaves were ground and mixed with manganese malate trihydrate previously synthesized in the following proportions: 10.34 g of leaves and 0.142 g of $MnC_4H_4O_5.3H_2O$ (0.59 mmol), which represents 0.31 wt% of Mn.

The mixture was thermally treated under air flow following the temperature program P1. Obtained ashes were then chemically activated following exactly the same procedure as the one used for Eco-Mn_1.

2.6. $KMnCl_3$ synthesis

The procedure followed is based on the one described by Horowits et al. [23]. 1.856 g of KCl (24.9 mmol, 1eq.) and 9.856 g of $MnCl_2.4H_2O$ (49.8 mmol, 2eq.) were added to a beaker and slowly dissolved in a 1 M HCl solution at ambient temperature. The solution was slowly evaporated at ambient temperature and atmospheric pressure, yielding $KMnCl_3.2H_2O$ pink crystalline needles. $KMnCl_3.2H_2O$ crystals were dried under vacuum (0.3 mbar) at 90 °C during 5 h, yielding anhydrous $KMnCl_3$.

2.7. $K_3NaMnCl_6$ synthesis

In a sealed tube, about 280 mg of Eco-Mn_1 and 1 mL of a 12 M HCl solution were introduced. The solution was stirred at 90 °C. HCl was slowly added to the sealed tube in order to completely dissolve Eco-Mn_1 catalyst in a minimum amount of 12 M HCl. Before each addition of HCl, the sealed tube was cooled at ambient temperature. Once Eco-Mn_1 had been completely dissolved, the mixture was slowly cooled with the following temperature program: 90-80 °C in 2 h, 80-65 °C in 1 h, 65-50 °C in one hour, 50-35 °C in one hour, and four days at ambient temperature. Two types of crystals were formed in the sealed tube: $K_3NaMnCl_6$ and $KMgCl_3.6H_2O$. Saltonseaite crystals, $K_3NaMnCl_6$, were easily isolated and stored under vacuum in a desiccator.

2.8. $MnHPO_4.3H_2O$ synthesis

The followed procedure is the one described by Wu et al. [24] to produce $Mn_3(PO_4)_2.3H_2O$. 6.761 g of $MnSO_4.H_2O$ (0.04 mol, 1eq.), 4.601 g of $NH_4H_2PO_4$ (0.04 mol, 1eq.), and 40 mL of deionised water were introduced in a round bottom flask. The mixture was stirred at ambient temperature to completely dissolve the salts. 100 mL of anhydrous ethanol was dropped into the pale pink solution under vigorous stirring. A pink precipitate was formed. The mixture was stirred 1 h. The pink solid was then filtered under vacuum, washed with 80 mL of deionised water, and dried in an oven at 80 C° during 18 h. The resulting solid was stored under vacuum in a desiccator. After XRD analysis, it appears that the formed solid was in fact $MnHPO_4.3H_2O$ (and not $Mn_3(PO_4)_2.3H_2O$).

2.9. $K_2FeCl_5.H_2O$ synthesis

The procedure is based on the one described by Falk et al. [25] and on the procedure used to produce $KMnCl_3$. 1.856 g of KCl (0.025 mol, 1eq.) and 13.461 g of $FeCl_3.6H_2O$ (0.050 mol, 2eq.) were added to a beaker. A 1 M HCl solution was slowly added under stirring at ambient temperature to dissolve the salts. The solution was slowly evaporated at ambient temperature and at atmospheric pressure. This yields red crystals of $K_2FeCl_5.H_2O$. Collected crystals were stored under vacuum in a desiccator.

2.10. Ref-Mn/anhydrous $MnCl_2$ synthesis

1.05 g (4.4 mmol) of manganese malate trihydrate was ground and thermally treated in an oven under air flow, following the temperature program P1. A fine black powder was obtained. This powder was chemically activated following exactly the same procedure, as the one used to produce Eco-Mn_1. Ref-Mn, under the form of pink powder, was stored under vacuum in a desiccator.

2.11. ICP-MS analysis

Precisely weighted samples were first digested in a mixture of hydrochloric acid (37%) (2 mL) and nitric acid (65%) (4 mL) using a microwave (Anton Paar Microwave GO), with the following temperature program: 20 °C—160 °C in 10 min and 10 min at 160 °C. Digested samples were then diluted to 0.05 mg L^{-1} in a nitric acid solution (1%). Three blanks were prepared following the previously described steps of digestion and dilution.

ICP-MS was performed on HR-ICP-MS Thermo Scientific Element XR apparatus. Three analyses were performed for each sample in order to determine the standard deviation of the measurement. Measures obtained with blank samples were averaged and subtracted to the measures obtained for each sample. Calibration was regularly checked.

2.12. XRD analysis

XRD data measurements were performed by using a BRUKER diffractometer (D8 advance, with a Cu Kα radiation $\lambda = 1.54086$ Å) equipped with a Lynxeye detector. Diffraction patterns were analyzed with DIFFRAC-EVA software and several XRD databases (Crystallography Open Data Base 2016, and PDF 2011, 2017 or 2018).

2.13. X-ray absorption spectroscopy

All the catalysts and reference samples were prepared under the form of pellets of 7-mm diameter. Catalysts under the form of powder were carefully mixed with cellulose powder, and ground, in order to prepare homogeneous pellets. Pellets were prepared in a glove box and then sealed in Kapton scotch.

XAS spectra at the Mn and Fe K edge were collected at SAMBA Beamline (Synchrotron SOLEIL) [26] equipped with a double-crystal Si 220 monochromator. Mn K-edge spectra were recorded in transmission mode with ionization chambers (IC-SPEC, FMB-Oxford), between 6300 and 7060 eV. Fe K-edge spectra were recorded in fluorescence mode with a 36-pixels Ge detector (Canberra) between 7000 and 7700 eV.

All samples were calibrated using a Mn (resp. Fe) foil during the experiments. Data analysis was performed using Demeter software package [27], as well as MAX software package [28,29]. The theoretical modelization and fit of the Extended X-Ray Absorption Fine Structure (EXAFS) spectra within Demeter software were done using crystallographic structures from two databases (COD [30] and The Materials Project [31]).

3. Results and discussion

3.1. Eco-Mn synthesis

Eco-Mn catalysts are produced in two main steps from Mn-enriched biomass (Fig. 1).

The experimental conditions are designed to develop Lewis acid properties in Eco-Mn, properties useful in many organic reactions. In order to characterize Eco-Mn, two parameters were varied: the

Fig. 1. Scheme presenting the different steps to produce Eco-Mn catalysts from Mn-accumulating plants' leaves.

nature of the plant species from which Eco-Mn catalysts were prepared and the concentration of HCl used to produce Eco-Mn catalysts (Table 1). Five endemic manganese (hyper)-accumulating plants have been used to produce Eco-Mn catalysts: four of them are currently used by our team to rehabilitate mining sites in New Caledonia, especially for their dryness, altitude, and low mineral supply resistance, *Grevillea exul* ssp. *exul*, *Grevillea exul* ssp. *rubiginosa*, *Grevillea meisneri*, and *Grevillea gillivrayi*. The fifth species, *Garcinia amplexicaulis*, is not used for ecological rehabilitation, but thanks to its outstanding Mn hyperaccumulation capacity; it constitutes an interesting candidate to establish correlations between plant's composition and ecocatalyst's structure (Fig. 2).

The same experimental method was used to produce all Eco-Mn catalysts, with variation only in the HCl concentration used (1 M, 4 M, or 12 M [Table 1]).

To reveal the vegetal footprint of Eco-Mn catalysts, we prepared two synthetic catalysts. We aimed to determine whether Eco-Mn catalysts can be reproduced, in terms of structure, properties, and catalytic activities, by mixtures of metallic salts.

Syn-Mn_1 was produced by mixing commercial metal chlorides, so that the relative percentages of metallic elements in Syn-Mn_1 and in *Grevillea exul* ssp. *rubiginosa* leaves are exactly the same (Fig. 3, SI appendix S1).

The selected metal chlorides to produce Syn-Mn_1 are $MnCl_2.4H_2O$, $MgCl_2$ (anhydrous), $CaCl_2$ (anhydrous), NaCl, KCl, $NiCl_2.6H_2O$, and $FeCl_3.6H_2O$ et $AlCl_3$ (anhydrous).

Syn-Mn_2 was synthesized in two steps. First, commercial or synthesized metallic salts were mixed together. Then, the mixture was thermally treated and chemically activated under the same experimental conditions as were the leaves of Mn-accumulating plants (SI Appendix S2).

Finally, a control catalyst, Tem-Mn, was also produced: leaves of *Grevillea rosa* subsp. *jenkinsii*, grown on a soil where manganese accumulation is not possible, were mixed with manganese malate trihydrate. Then, the mixture was thermally treated and chemically activated under the same conditions as those used for Mn-accumulating plants. Tem-Mn was designed to test whether Eco-Mn can be reproduced by mixing biomass with a manganese salt.

Table 1
Table summarizing the different Eco-Mn catalysts that have been produced in this study, the plants they originate from, and the concentrations of the HCl solution in the process.

	Chemical activation (HCl)		
	HCl 12 M	HCl 4 M	HCl 1 M
Grevillea exul ssp. *rubiginosa*	Eco-Mn_1	Eco-Mn_6	Eco-Mn_9
Grevillea exul ssp. *exul*	Eco-Mn_2	/	/
Grevillea gillivrayi	Eco-Mn_3	/	/
Grevillea meisneri	Eco-Mn_4	Eco-Mn_7	/
Garcinia amplexicaulis	Eco-Mn_5	Eco-Mn_8	Eco-Mn_{10}

3.2. ICP MS analyses

Metallic composition of Mn-accumulating plants, of ashes resulting from the thermal treatment, and of Eco-Mn, Syn-Mn, and Tem-Mn catalysts was studied by ICP-MS analyses (Table 2, SI Appendix S3).

The results show that Eco-Mn catalysts are made up of manganese (2.5 wt% to 12.5 wt% [dry weight]), calcium (Ca), magnesium (Mg), sodium (Na), potassium (K), and iron (Fe) (0.3 wt% to 3 wt% [dry weight]). These latter five elements are necessary for plant growth and are thus present in resulting Eco-Mn. Finally, Eco-Mn catalysts contain traces of aluminum and nickel. Recent advances in chemistry have elucidated the key role of iron in catalysis [32,33], and the combined presence of iron and manganese in Eco-Mn may be a huge asset in considerations of future organic syntheses.

The histogram Fig. 4 shows relative weight percentages of metallic elements in Eco-Mn, Syn-Mn, and Tem-Mn catalysts.

When Eco-Mn catalysts obtained from a single plant species are compared, it is clear that Eco-Mn catalysts activated with HCl 12 M and 4 M have quite similar elemental compositions (Eco-Mn_1 and Eco-Mn_6; Eco-Mn_4 and Eco-Mn_7; and Eco-Mn_5 and Eco-Mn_8) and that composition of Eco-Mn activated with HCl 1 M (Eco-Mn_9; Eco-Mn_{10}) is different, especially regarding manganese concentration. A 1 M HCl solution is not concentrated enough to react properly with manganese oxides in the ash.

Differences in the chemical compositions appear between catalysts prepared from different plant species: accumulating properties are specific to each plant species and the elemental composition of resulting Eco-Mn catalysts reflects the Mn accumulation capacity of the source plant. In other words, the heritage of the complex chemical composition of Eco-Mn catalysts from their source plant is one part of what we call their 'vegetal footprint'. This is supported by differences between Eco-Mn_1 and Tem-Mn compositions: New Caledonian plants give a specific chemical composition to Eco-Mn catalysts that cannot be reproduced by adding Mn malate salt to biomass from *Grevillea rosa* subsp. *jenkinsii*.

Interestingly, metallic compositions of Syn-Mn_1 and Eco-Mn_1 are different (SI Appendix S3-Table S2). Therefore, it clearly appears that a mixture of simple chloride salts does not reproduce properly the elemental composition of an Eco-Mn catalyst. Concerning Syn-Mn_2, its chemical composition is closer to that of Eco-Mn_1, taking into account uncertainties, except for calcium and magnesium concentrations. Repeatedly producing an ecocatalyst with the same elemental composition is not simple, even when the initial salt mixture used to produce Syn-Mn_2 is subject to the same experimental conditions as Mn-rich biomass.

3.3. XRD experiments

Eco-Mn catalysts in the form of powder, as well as ashes resulting from the thermal treatment of either Mn-accumulating plants or mixtures of metallic salts, were analyzed by XRD. Two

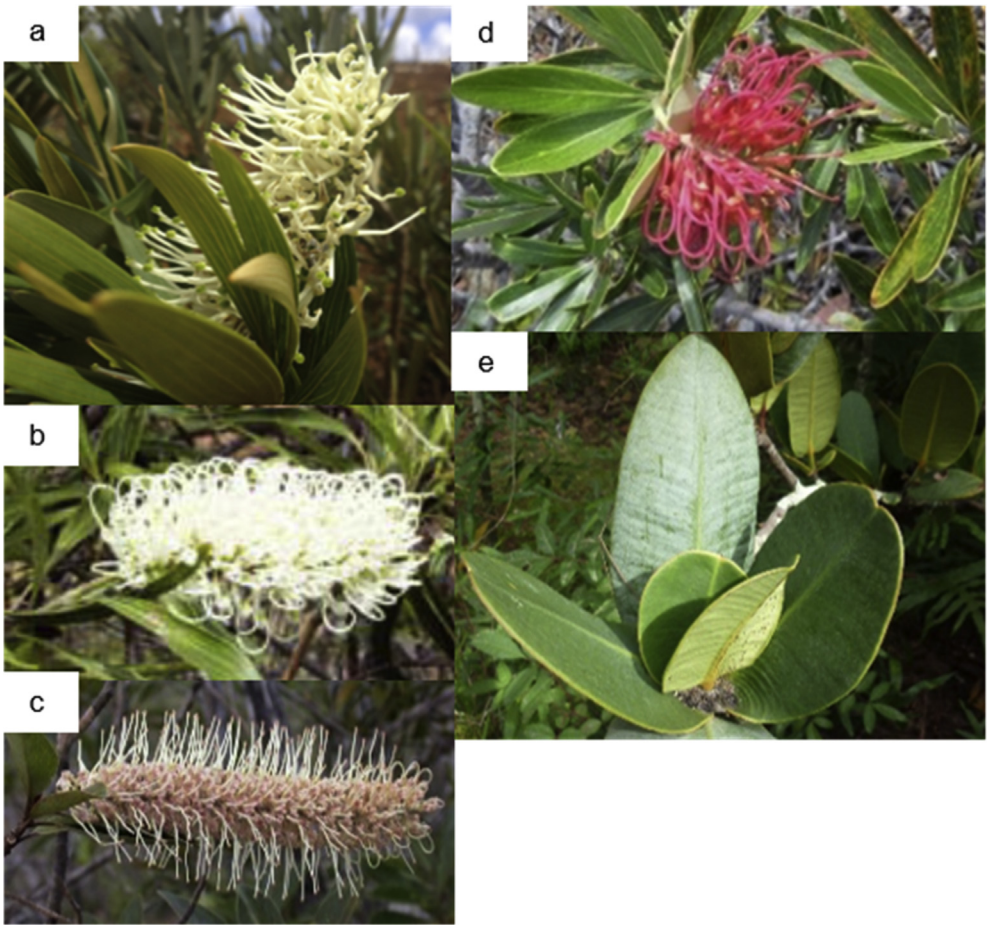

Fig. 2. Photographs of the five manganese (hyper)-accumulating plants used to produce Eco-Mn catalysts: (a) *Grevillea exul* ssp. *rubiginosa*; (b) *Grevillea exul* ssp. *exul*; (c) *Grevillea gillivrayi*; (d) *Grevillea meisneri*, and (e) *Garcinia amplexicaulis*.

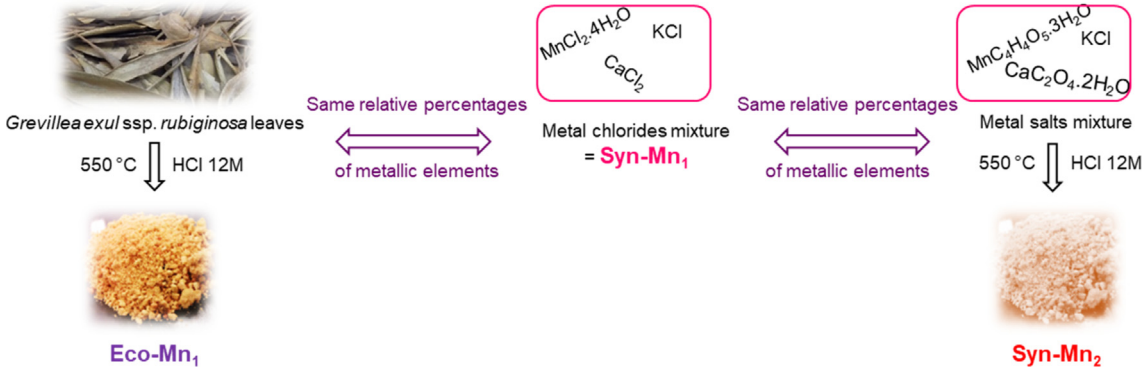

Fig. 3. Scheme presenting the synthetic catalysts Syn-Mn_1 and Syn-Mn_2.

examples of the typical diffraction patterns are presented in SI Appendix S4. Identified crystalline phases are summarized for each catalyst in Table 3.

In Eco-Mn, XRD highlights the presence of simple metal chlorides such as $CaCl_2$, or $MnCl_2.2H_2O$, but above all, the presence of mixed metal chlorides such as $K_3NaMnCl_6$, $KMnCl_3$, and $KMgCl_3.6H_2O$. The presence of $K_3NaMnCl_6$ was also proved by recrystallizing an Eco-Mn catalyst in 12 M HCl solution at 90 °C (Fig. 5).

Although the crystal structure of these mixed salts is reported in the literature [34,35], nothing is reported regarding their catalytic potential in organic synthesis. Everything remains to be studied, and ongoing research in our team aims at defining their catalytic activity. For instance, $KMgCl_3.6H_2O$ has recently been demonstrated to show unique catalytic activity, even better than that achieved with $MgCl_2$ in Knoevenagel reactions [36]. This suggests the interest of evaluating the synthetic potential of $KMnCl_3$, $K_3NaMnCl_6$, and $KMgCl_3.6H_2O$. First results are given in the section 'DFT calculations of mixed Mn salts'.

It should be noted that manganese crystalline species identified in Eco-Mn and in Syn-Mn_2 catalysts are different. Diffraction peaks

Table 2
Elemental composition of Mn-accumulating plants' leaves, ashes, Eco-Mn, Syn-Mn, and Tem-Mn catalysts determined by ICP-MS analysis.

		Na	Mg	Al	K	Ca	Mn	Fe	Ni
Leaves, *Grevillea exul* ssp. *rubiginosa*	ppm	1207	2408	172	4406	2354	4023	492	109
	RSD (%)	1.045	0.54	0.803	2.224	1.284	0.706	1.605	0.703
Ashes, *Grevillea exul* ssp. *rubiginosa*	ppm	37333	76667	4270	130991	72342	127496	10054	2973
	RSD (%)	0.50	0.70	6.10	0.28	1.18	0.39	0.51	0.49
Eco-Mn_1, *Grevillea exul* ssp. *rubiginosa*. HCl 12 M	ppm	8128	54353	2914	37857	78575	64570	7206	2034
	RSD (%)	1.11	1.37	1.02	1.27	0.07	0.56	0.46	0.44
Eco-Mn_6, *Grevillea exul* ssp. *rubiginosa*. HCl 4 M	ppm	20885	39889	2560	71092	86711	68310	6700	1601
	RSD (%)	3.57	4.07	3.75	0.26	0.55	0.96	0.85	0.41
Eco-Mn_9, *Grevillea exul* ssp. *rubiginosa*. HCl 1 M	ppm	24746	50787	3652	83498	104582	32728	7478	1926
	RSD (%)	0.58	0.80	0.25	1.14	1.01	1.19	1.35	0.23
Leaves, *Grevillea exul* ssp. *exul*	ppm	514	1828	30	7139	8594	2191	1192	146
	RSD (%)	1.89	1.65	1.44	1.20	1.38	1.25	1.44	1.44
Ashes, *Grevillea exul* ssp. *exul*	ppm	13640	40511	2235	138231	178146	58262	33827	3269
	RSD (%)	3.70	3.34	3.69	1.03	0.80	0.58	0.60	0.29
Eco-Mn_2, *Grevillea exul* ssp. *exul*. HCl 12 M	ppm	5815	32704	1731	98708	99751	39994	27733	2577
	RSD (%)	2.03	1.74	0.78	0.77	0.97	0.75	0.49	0.51
Leaves, *Grevillea gillivrayi*	ppm	1162	3069	482	2771	11477	3606	2368	62
	RSD (%)	1.57	1.11	1.19	0.65	0.39	0.37	0.72	0.76
Ashes, *Grevillea gillivrayi*	ppm	17992	80892	4217	53705	189643	87080	37153	1606
	RSD (%)	2.22	2.23	2.09	1.11	0.49	0.53	0.95	0.45
Eco-Mn_3, *Grevillea gillivrayi*. HCl 12 M	ppm	6174	49642	2236	31149	99979	55113	21568	976
	RSD (%)	3.86	3.14	4.08	2.26	2.59	2.08	2.56	2.50
Leaves, *Grevillea meisneri*	ppm	1378	1233	0	2746	8041	6690	63	30
	RSD (%)	5.63	5.70	7.17	0.58	1.11	0.28	0.25	0.72
Ashes, *Grevillea meisneri*	ppm	24743	29213	747	56405	182353	190720	3270	718
	RSD (%)	0.79	0.39	2.12	0.38	0.64	0.75	0.91	1.04
Eco-Mn_4, *Grevillea meisneri*. HCl 12 M	ppm	8414	20108	1637	39377	125405	117155	3738	483
	RSD (%)	6.44	5.10	4.87	0.84	0.40	0.45	1.01	1.33
Eco-Mn_7, *Grevillea meisneri*. HCl 4 M	ppm	14890	18120	730	33202	120716	114194	2592	460
	RSD (%)	3.22	3.08	4.45	0.45	0.42	0.41	0.17	1.15
Leaves, *Garcinia amplexicaulis*	ppm	600	3821	0	320	10773	8759	147	108
	RSD (%)	2.10	1.91	1.19	0.90	0.18	0.19	0.66	0.18
Ashes, *Garcinia amplexicaulis*	ppm	19283	61985	794	9938	199344	203915	8366	2334
	RSD (%)	0.87	0.71	2.15	0.93	0.50	0.67	0.89	0.64
Eco-Mn_5, *Garcinia amplexicaulis*. HCl 12 M	ppm	7453	38575	848	8550	99401	126236	5061	1445
	RSD (%)	2.40	2.25	3.57	0.87	0.92	0.87	3.69	2.16
Eco-Mn_8, *Garcinia amplexicaulis*. HCl 4 M	ppm	10437	35812	555	8077	115443	103216	3991	1240
	RSD (%)	1.48	1.59	2.15	0.95	0.72	0.32	0.62	0.87
Eco-Mn_{10}, *Garcinia amplexicaulis*. HCl 1 M	ppm	15546	50955	437	8217	139190	26056	2589	1531.94
	RSD (%)	1.36	1.21	1.47	1.14	0.82	0.96	0.62	0.87
Syn-Mn_1, synthetic catalyst	ppm	26765	35381	2044	77030	48293	69553	8056	1509
	RSD (%)	1.96	1.66	2.04	0.86	1.18	1.00	0.78	0.86
Syn-Mn_2, starting salt mixture	ppm	21003	41846	1694	70652	34573	85958	7240	2001
	RSD (%)	0.78	0.54	1.14	0.51	1.87	0.38	0.60	0.73
Syn-Mn_2, ashes	ppm	31030	64049	2228	106734	51279	134279	10773	2382
	RSD (%)	1.65	1.71	2.67	1.15	2.02	1.09	1.24	1.13
Syn-Mn_2, synthetic catalyst	ppm	9388	32953	1193	47058	30515	64340	5474	1400
	RSD (%)	0.24	0.30	1.67	0.74	1.74	0.36	0.27	0.37
Leaves, *Grevillea rosa* ssp. *jenkinsii*	ppm	122	2390	0	4051	17640	920	4	1
	RSD (%)	2.77	2.60	1.89	0.82	1.21	1.32	1.36	1.91
Ashes, *Grevillea rosa* ssp. *jenkinsii* + $MnC_4H_4O_5.3H_2O$	ppm	11290	54344	787	90355	437313	57359	1555	32
	RSD (%)	2.06	2.13	0.58	0.23	0.86	0.83	3.52	5.58
Tem-Mn, *Grevillea rosa* ssp. *jenkinsii* + $MnC_4H_4O_5.3H_2O$. HCl 12 M	ppm	1530	23634	535	40634	179724	39273	720	12
	RSD (%)	3.89	3.14	2.97	3.10	2.74	3.04	4.12	16.37

ICP-MS, inductively coupled plasma mass spectrometry, RSD, Relative Standard Deviation.

of $MnMg_2Cl_6.12H_2O$ are clearly identified with Syn-Mn_2 catalyst, while this species is not present, at least not in crystalline form, in Eco-Mn. Likewise, $KMnCl_3$ and $K_3NaMnCl_6$, both clearly identified in Eco-Mn catalysts, are not observed in the Syn-Mn_2 diffraction pattern. Thus, it appears that Eco-Mn and Syn-Mn catalysts do not crystallize in the same way, even though Syn-Mn_2 and Eco-Mn_1 have relatively close metallic compositions. It is well known that crystallinity of metallic compounds might have a significant impact on their catalytic potential, as is the case for MnO_2, for instance Refs. [37,38]. Thus, the different crystalline species in Eco-Mn and in Syn-Mn might impact their catalytic properties. Studies examining this question are currently ongoing.

Regarding ash, the mixed calcium manganese oxide $Ca_2Mn_3O_8$ is present in ash from several Mn-accumulating plants (Table 4).

This should be proven by another analytical method, such as XAS, but this identification could be anticipated since Vassilev et al. have reported this oxide among species present in ash from non-accumulating plants [39]. The same crystalline species is absent in ash resulting from the thermal treatment of the mixture of salts Syn-Mn_2: this highlights again a significant difference between 'eco-ashes' and 'synthetic ashes'. It seems that the complex composition of plants leads to different crystallization mechanisms. Furthermore, several articles in the literature report the benefits of mixed calcium manganese oxides such as $Ca_2Mn_3O_8$, especially for water oxidation reactions [40], but preparation of such mixed oxides is complex [40–42]. Here, we report for the first time that a simple and environmentally friendly thermal treatment of Mn-rich biomass from New Caledonia seems to produce $Ca_2Mn_3O_8$. This

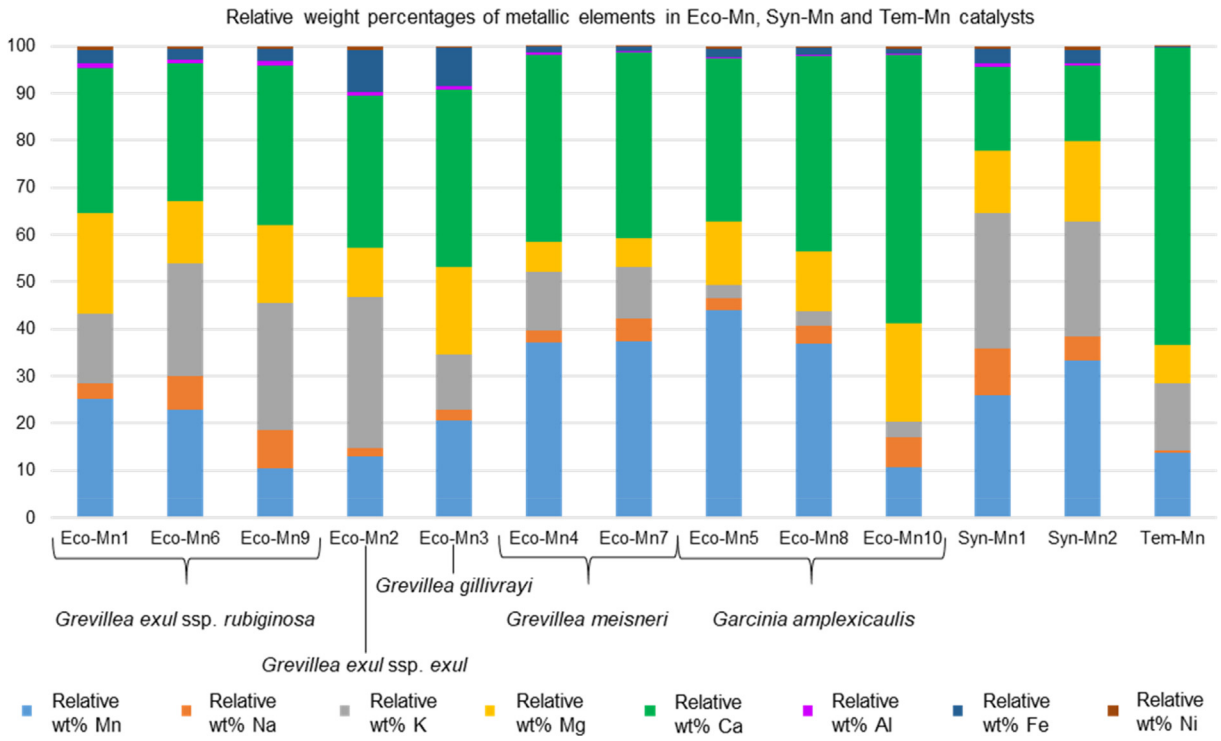

Fig. 4. Histogram presenting the relative weight percentages of metallic elements in Eco-Mn, Syn-Mn, Tem-Mn catalysts.

Table 3
Summary of crystalline species identified in Eco-Mn, Tem-Mn, and Syn-Mn catalysts.

	$MnCl_2.2H_2O$	$KMnCl_3$	$K_3NaMnCl_6$	$MnMg_2Cl_6.12H_2O$	$CaCl_2$ anhydrous	$CaCl_2.2H_2O$	$CaCl_2.4H_2O$	$CaMg_2Cl_{6.\ 12H2O}$	$KMgCl_3.6H_2O$	$MgCl_2.6H_2O$	$CaSO_4.xH_2O$[a]	NaCl
Eco-Mn_1		✓	?			✓		✓			?	
Eco-Mn_6		?	✓				✓	✓			✓	
Eco-Mn_9		?	✓				?	✓	✓		✓	✓
Eco-Mn_2		?	✓			✓		✓			?	
Eco-Mn_3		✓	?			✓						✓
Eco-Mn_4	✓	✓				✓		✓				✓
Eco-Mn_7		✓			✓	✓						✓
Eco-Mn_5	✓					✓		✓				✓
Eco-Mn_8	✓		?			✓					✓	✓
Eco-Mn_{10}							✓	✓			✓	
Tem-Mn								✓				
Syn-Mn_2				✓							✓	

XRD, X-ray diffraction.
Question marks indicate that the corresponding species might be present in the catalyst but cannot be identified with certainty on the XRD pattern.
[a] $CaSO_4.xH_2O$ regroups all the calcium sulfate species more or less hydrated.

may pave the way to the exploration of new catalysts of oxidation reactions.

3.4. X-ray absorption spectroscopy

XRD analyses do not allow the identification of non-crystalline species in Eco-Mn. It was thus necessary to get access to the local environment around the candidate active catalytic elements: manganese and iron. Therefore, Eco-Mn, Syn-Mn, and Tem-Mn catalysts have been studied by XAS.

XAS is an increasingly frequently used technique to determine the geometric and electronic structure around a given element independently of the existence or not of long-range order. X-ray absorption spectra of Eco-Mn, Syn-Mn, and Tem-Mn were measured at the Mn K-edge and at the Fe K-edge (Fig. 6). All the experiments were performed at the SOLEIL Synchrotron, on SAMBA beamline [23].

The analysis of XAS is facilitated by comparison with the spectra of reference compounds whose crystallographic structures are well known. Thus, thirteen manganese and iron salts have been carefully selected as references (SI Appendix S5). Some of these salts were synthesized in the laboratory, and their structure was checked, either by XRD analyses or by XAS simulation.

The pre-edge peak intensity of transition metal K-edge spectra depends on the site symmetry: almost null in a perfect octahedron, it rises slightly with octahedron distortions and increases significantly for tetrahedral sites. The energy position of the pre-edge increases for higher metal oxidation states and shorter metal–ligand bond lengths [43–47]. Therefore, both the pre-edge peak energy and intensity were used to characterize the oxidation states and local symmetries of Mn and Fe complexes in catalysts (Fig. 7).

The Mn K pre-edge energy and intensity of XAS spectra of all studied catalysts are very close to those of $KMnCl_3$ and $MnCl_2.2H_2O$.

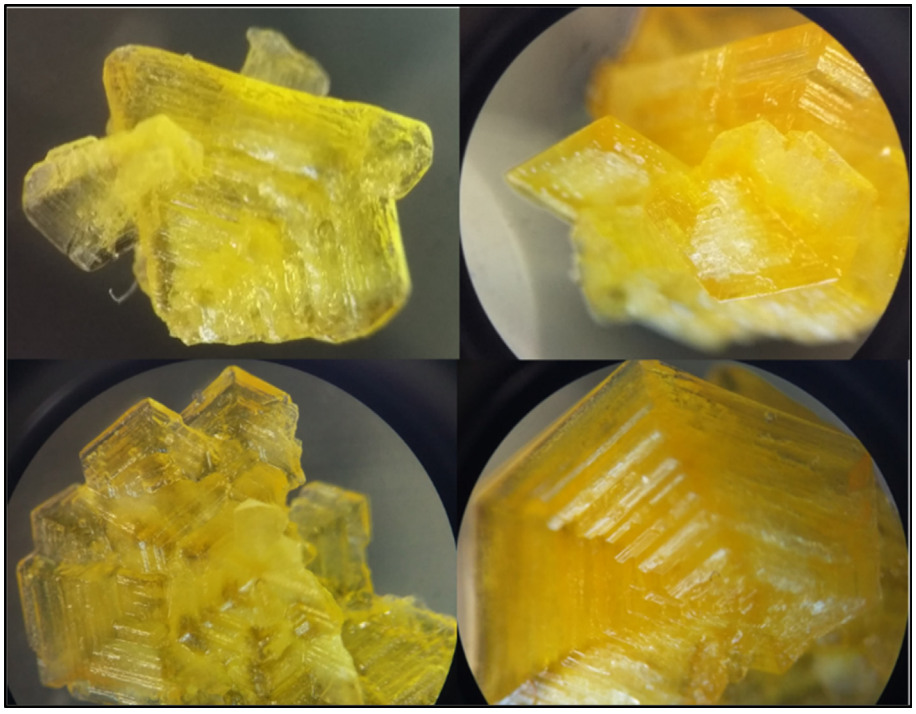

Fig. 5. Optic microscopic observations of saltonseaite $K_3NaMnCl_6$ crystals. (Optic microscope Paralux, magnification factor X40).

Table 4
Summary of crystalline species identified in ashes resulting from the thermal treatment of Mn-accumulating plants, the thermal treatment of *Grevillea rosa* ssp. *jenkinsii* with manganese malate trihydrate and the thermal treatment of metallic salts mixture.

	$CaCO_3$	KCl	$Ca_2Mn_3O_8$	Mg_6MnO_8	Mn_2O_3	K_2SO_4	$K_3Na(SO_4)_2$
Ashes *Grevillea exul* ssp. *rubiginosa*	✓	✓	✓	✓			✓
Ashes *Grevillea exul* ssp. *exul*	✓	✓				✓	
Ashes *Garcinia amplexicaulis*	✓		✓				
Ashes *Grevillea gillivrayi*	✓	✓	✓				✓
Ashes *Grevillea meisneri*	✓	✓	✓				✓
Ashes *Grevillea rosa* ssp. *jenkinsii*	✓	✓					
Ashes Syn-Mn_2		✓			✓		

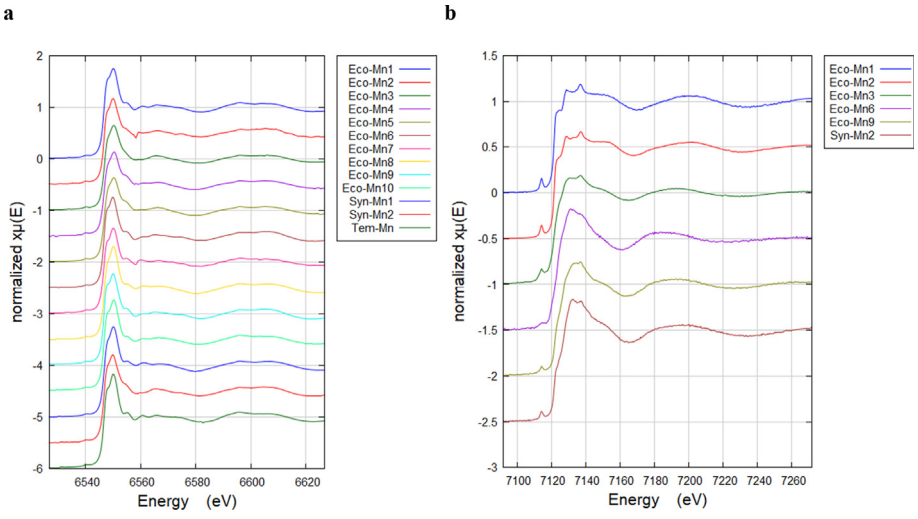

Fig. 6. Normalized X-ray absorption spectra of Eco-Mn, Tem-Mn, and Syn-Mn catalysts at (a) the Mn K-edge and at (b) the Fe K-edge.

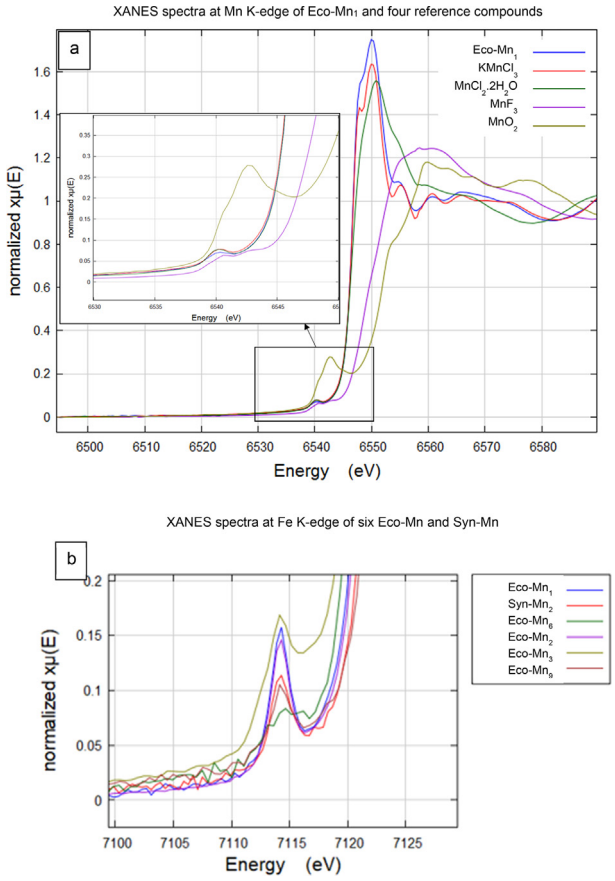

Fig. 7. X-ray Absorption Near Edge Structure (XANES) spectra at (a) Mn K-edge and (b) Fe K-edge of some Eco-Mn and Syn-Mn catalysts and some reference compounds.

Therefore, it appears that Mn is only present under the oxidation state Mn(II) in Eco-Mn, Tem-Mn and Syn-Mn, and exclusively in an octahedral environment. Comparing the Fe K pre-edge energy observed on spectra of the studied catalysts and on spectra of reference compounds, it is clear that iron is mainly under the oxidation state Fe(III) in Eco-Mn, Syn-Mn and Tem-Mn catalysts. Comparing Fe K pre-edge intensity observed on spectra of the studied catalysts, and considering the indications of Wilke et al. [46], it appears that Eco-Mn_6, Eco-Mn_9, and Syn-Mn_2 are most likely composed of octahedral iron complexes, while Eco-Mn_1, Eco-Mn_2, and Eco-Mn_3 at least partly contain iron in tetrahedral geometry.

Eco-Mn catalysts comprise not only a single pure manganese species but also mixtures of several pure manganese species. That is why EXAFS spectra cannot be easily fitted to determine the nature and the structure of manganese species composing Eco-Mn catalysts. Therefore, principal component analysis (PCA) was performed using MAX-Straight No Chaser software [28,29] (SI Appendix S6). It seems that Eco-Mn catalysts are mainly composed of six manganese species. In addition, Target Transformation (SI Appendix S6) clearly shows that the reference compounds most likely to be present in Eco-Mn, Syn-Mn, and Tem-Mn catalysts are chlorinated species, such as $MnCl_2$, $MnCl_2.2H_2O$ $KMnCl_3$, $K_3NaMnCl_6$, and $MnMg_2Cl_6.12H_2O$. Oxygen-rich manganese species are unlikely to be present, along with manganese sulfate or phosphate.

PCA was followed by a linear combination fitting (LCF) in order to determine the nature and proportions of Mn species in each studied catalyst. LCF was performed by using Athena software [28] and spectra of the reference compounds selected with the Target Transformation (SI Appendix S7).

For some catalysts, the LCF spectra are very close to the experimental spectra, as it is the case for Eco-Mn_4. In other cases, comparison of LCF spectra and experimental spectra suggests that a component might remain to be identified as in Eco-Mn_9 (Fig. S8), which means that one manganese species is unidentified. LCF analysis gives valuable qualitative information concerning the composition of Eco-Mn, Syn-Mn, and Tem-Mn catalysts (SI Appendix S7): main Mn species that comprise the different catalysts are now clearly identified, as summarized in Table 5, which to the best of our knowledge has never been done before. Furthermore, XAS analysis highlights the presence of $MnMg_2Cl_6.12H_2O$ in several Eco-Mn catalysts, which has never been observed in XRD patterns.

Thus, XAS analyses corroborate and extend results of the XRD analyses. Mixed chloride salts are identified in Eco-Mn and Syn-Mn catalysts, but their relative abundances differ depending on the catalysts, probably due to their different elemental composition.

Concerning Fe K-edge spectra, PCA analyses were not possible as the number of recorded spectra was too small. XAS Fe K-edge spectra of Eco-Mn_1 show a particular shape, which corresponds to several reported XAS spectra of species under the form: $[A^+, FeCl_4^-]$ [47,48,49] (SI Appendix S8). Studies to identify the nature of the A^+ cation in Eco-Mn_1 are ongoing, but this result is in accordance with the tetrahedral geometry previously highlighted by XANES study.

Taking the Eco-Mn_1 spectrum as a 'pseudo-reference' compound, LCF was performed on XANES Fe K-edge spectra of the other studied catalysts (SI Appendix S9). Eco-Mn_2 and Eco-Mn_3 probably contain a $[A^+, FeCl_4^-]$ species, which is coherent with the XANES study. Some differences between experimental and LCF spectra (such as for Eco-Mn_6) indicate that some Fe-rich species remain to be identified, but this study gives, for the first time, insight into the chemical environment around iron atoms in Eco-Mn, which was not possible by previously used analytical methods. As for Mn species, the catalytic potential of identified iron salts, such as $K_2FeCl_5.H_2O$, has not been explored and opens up new possibilities in iron catalysis.

It appears that Syn-Mn_2 probably contains $FePO_4.2H_2O$, which is logical as the latter is used as starting material for its synthesis. As already observed for Mn, it appears that the chemical environment around Fe in Eco-Mn_1 catalyst differs from that in its synthetic counterpart Syn-Mn_2.

3.5. DFT calculations of mixed Mn salts

All calculations were performed in the ground state ($S = 1/2$), using three solvation systems (water, acetone, and tetrahydrofuran) with rather specific dipolar moments in order to reproduce different experimental conditions used in organic synthesis (SI Appendix S10). Evaluation of the atomic charges held by the manganese catalytic center was done using several methods (Mulliken, Natural bond orbital and Merz-Singh-Kollman). They all have revealed significant variation in the charge present on Mn depending on the composition of salts (Table 6).

Indeed, the distribution of the positive charges and particularly on the Mn atom differs in most cases by more than 100% between $MnCl_2$ and $K_3NaMnCl_6$. These electronic variations surely imply significant differences concerning the electrophilic properties of the metal cations and hence probably as well of the Lewis acid properties. The softness of the mixed salts was also evaluated and revealed some fluctuations depending on the solvents. Independently of the solvent, $KMnCl_3$ displays the softest character.

Table 5
Summary of Mn-rich species identified in each catalyst with XAS analysis (PCA and LCF) and with XRD analysis.

	LCF analysis on XANES spectra (main Mn-rich species)	XRD analysis (crystalline Mn-rich species)
Eco-Mn_1	$K_3NaMnCl_6$	$KMnCl_3$ (Eco-Mn_1)
Eco-Mn_6	$KMnCl_3$ (minor in Eco-Mn_9)	$K_3NaMnCl_6$ (Eco-Mn_6 and EcoMn_9)
Eco-Mn_9	Anhydrous $MnCl_2$	
Eco-Mn_{10}		
Tem-Mn	$KMnCl_3$	/
	Anhydrous $MnCl_2$	
Eco-Mn_3	$MnMg_2Cl_6.12H_2O$	$MnCl_2.2H_2O$ (Eco-Mn_4 and EcoMn_5)
Eco-Mn_4	$MnCl_2.2H_2O$	$KMnCl_3$ (Eco-Mn_3 and Eco-Mn_4)
Eco-Mn_5	Anhydrous $MnCl_2$ ($K_3NaMnCl_6$ in Eco-Mn_4)	
Eco-Mn_8	Anhydrous $MnCl_2$	$MnCl_2.2H_2O$
Syn-Mn_1	Anhydrous $MnCl_2$	
	$KMnCl_3$	
Syn-Mn_2	$K_3NaMnCl_6$	$MnMg_2Cl_6.12H_2O$
	Anhydrous $MnCl_2$	
	$MnMg_2Cl_6.12H_2O$	
Eco-Mn_2	$K_3NaMnCl_6$	$K_3NaMnCl_6$
	$KMnCl_3$	
	Anhydrous $MnCl_2$	
	$MnMg_2Cl_6.12H_2O$	
Eco-Mn_7	$KMnCl_3$	$KMnCl_3$
	Anhydrous $MnCl_2$	

XAS, X-ray absorption spectroscopy; PCA, principal component analysis; LCF, linear combination fitting; XRD, X-ray diffraction.
Eco-Mn_2 and Eco-Mn_7 are indicated in grey as for both of them, LCF analysis cannot be performed precisely because their XAS spectra are noisy.

Table 6
Results of DFT analysis of Mn salts.

Solvent		Water			Acetone			Tetrahydrofurane		
Mn salt		$MnCl_2$	K**Mn**Cl_3	K3Na**Mn**Cl_6	$MnCl_2$	K**Mn**Cl_3	K_3Na**Mn**Cl_6	$MnCl_2$	K**Mn**Cl_3	K3Na**Mn**Cl_6
Mn	Mulliken	−0.086	0.425	3.374	−0.093	0.390	3.385	−0.110	0.350	3.513
	NBO	0.565	0.482	0.02	0.560	0.482	0.238	0.549	0.482	0.195
	MK	1.215	1.00	0.570	1.243	1.100	0.573	1.221	1.103	0.607
Charges on K		–	**K**$MnCl_3$	**K_3**$NaMnCl_6$	–	**K**$MnCl_3$	**K_3**$NaMnCl_6$	–	–	**K_3**$NaMnCl_6$
K	Mulliken	–	0.860	0.729	–	0.850	0.717	–	0.826	0.684
	NBO	–	0.940	0.889	–	0.937	0.888	–	0.929	0.881
Charges on Na		–	–	K3**Na**$MnCl_6$	–	–	K_3**Na**$MnCl_6$	–	–	K_3**Na**$MnCl_6$
Na	Mulliken	–	–	0.638	–	–	0.620	–	–	0.576
	NBO	–	–	0.890	–	–	0.887	–	–	0.876
Solvent		water			acetone			tetrahydrofurane		
Mn salt		$MnCl_2$	K**Mn**Cl_3	K_3Na**Mn**Cl_6	$MnCl_2$	K**Mn**Cl_3	K_3Na**Mn**Cl_6	$MnCl_2$	K**Mn**Cl_3	K_3Na**Mn**Cl_6
Alpha occ. Eigenvalues		−0.20962	−0.21781	−0.21699	−0.21547	−0.2172	−0.21726	−0.21404	−0.21574	−0.21219
Alpha virt. eigenvalues		−0.04088	−0.03441	−0.03969	−0.03791	−0.03394	−0.03998	−0.03861	−0.03304	−0.03521
ɲ (hardness)		0.169	0.183	0.77	0.178	0.183	0.177	0.175	0.183	0.177
S (Softness)		**5.93**	**5.45**	**5.64**	**5.63**	**5.46**	**5.64**	**5.70**	**5.47**	**5.65**

Additionally, while the softness of $KMnCl_3$and $K_3NaMnCl_6$ was solvent independent, $MnCl_2$ has shown larger difference depending on the solvation environment. It is very interesting to investigate those new mixed salts using ab initio techniques in order to access some information sometimes difficult to obtain experimentally and of course to help understand the trends obtained experimentally. Furthermore, theory can allow a rapid screening of the potential of these new salts as catalysts in organic chemistry. For a deeper analysis of the physicochemical properties (spectroscopic, magnetic, and energetic) of the metallic salts, comparison of low- and high-spin configurations will be performed and reported shortly. The tandem of experimental and theoretical techniques can reveal to be very powerful in the quest of new bioinspired catalytic agents.

4. Conclusions

For the first time, we have described the unusual structure and composition of Eco-Mn catalysts. Eco-Mn catalysts are polymetallic catalysts, with Mn and Fe, respectively, under oxidation states II and III. ICP-MS and XAS data were overlapped (SI Appendix S11), and it appears that results are overall coherent (only potassium content inferred from LCF analysis is a bit high in some catalysts compared to ICP-MS analysis). For the first time, main Mn species which comprise Eco-Mn catalysts have been identified. Some similarities appear between catalysts which originate from the same plant species, which seems logical (SI Appendix S13). To further explain XAS results, all the metallic cations which comprise Eco-Mn have to be taken into account because they associate in various polymetallic salts.

Furthermore, XAS data are in accordance with XRD analyses for Eco-Mn_1, Eco-Mn_2, Eco-Mn_5 to Eco-Mn_{10}, Syn-Mn, and Tem-Mn. In Eco-Mn_3 and Eco-Mn_4, $KMnCl_3$ has been clearly identified on XRD patterns, but it is excluded or negligible in XAS LCF analysis; XAS is sensitive to all Mn atoms in the sample disregarding their long-range order, but easily misses minority phases, while XRD requires long-range order (crystallinity) and could miss amorphous

or nanophases. This result should be better interpreted in the frame of the complementarity of the two techniques and the necessity of using both for so complex specimens.

Several unexpected mixed salts were identified ($K_3NaMnCl_6$, $KMnCl_3$, $MnMg_2Cl_6.12H_2O$, and $K_2FeCl_5.H_2O$), by XRD analyses first and/or by XAS studies, and that has been done regarding manganese and iron. The catalytic potential and the specific Lewis acidity of these salts still have to be confirmed, but all the previous results suggest new opportunities for catalysis in organic synthesis. Several ongoing DFT studies in our group highlight the Lewis acid potential of these mixed manganese salts. Lewis and Brønsted acidity studies will direct the choice of Eco-Mn catalysts depending on the organic reaction affected. In addition, presence of hydrated salts in Eco-Mn catalysts has already proven to be an asset in some organic syntheses, such as in reductive aminations [7].

Eco-Mn specificity has been highlighted by comparing Syn-Mn and Tem-Mn catalysts. ICP-MS, XRD, and XAS analyses clearly show that contrary to Syn-Mn_1, Eco-Mn catalysts are not a juxtaposition of simple metal chlorides, and their composition is much more complex. The crystallinity of Mn and Fe species are different in Eco-Mn and Syn-Mn_2. We can assume that Eco-Mn compounds have a vegetal footprint in terms of their elemental composition and because crystallization pathways are not the same in Eco-Mn and Syn-Mn. This has to be taken into account to study their catalytic activity.

Finally, this structural study highlights the originality of these biosourced Eco-Mn catalysts, providing a better insight of their structure and their properties, which is necessary to consider and explain their catalytic activity in further organic reactions. Besides, all these results open a wide range of potentiality to explore new catalytic species in green and sustainable chemistry. Hence, these results may be regarded as door-openers for yet-to-be-expected next steps in this field of bioinspired catalysis.

Acknowledgments

The authors acknowledge CNRS, Stratoz, Société Le Nickel (SLN) and Koniambo Nickel SA (KNS) for your financial supports, SOLEIL for provision of synchrotron radiation facilities, and they would like to thank Karine Chaouchi for assistance in preparing our samples in the chemistry laboratory. We also thank Franck Pelissier, Gorka Gorazureta and Camille Bihanic for their help in performing experiments at Synchrotron SOLEIL, Christophe Cartier dit Moulin for his advices in XAS and Doyle McKey for his re-reading of the article and English corrections. The authors are grateful to the South and North Provinces of New Caledonia for their authorizations.

Appendix A. Supplementary data

Supplementary data to this article can be found online at https://doi.org/10.1016/j.mtsust.2019.100020.

References

[1] E. van der Voet, R. Salminen, M. Eckelman, T. Norgate, G. Mudd, R. Hisschier, J. Spijker, M. Vijver, O. Selinus, L. Posthuma, D. de Zwart, D. van de Meent, M. Reuter, L. Tikana, S. Valdivia, P. Wäger, M.Z. Hauschild, A. de Koning, Environmental Challenges of Anthropogenic Metals Flows and Cycles, United Nations Environment Programme, 2013.
[2] N. Myers, Threatened biotas: “Hot spots” in tropical forests, Environmentalist 8 (1988) 187–208.
[3] A. Garces-Granda, G.T. Lapidus, O.J. Restrepo-Baena, The effect of calcination as pre treatment to enhance the nickel extraction from low-grade laterites, Miner. Eng. 120 (2018) 127–131.
[4] B. Robineau, L. Berthault, P. Christmann, Nouvelle-Calédonie, terre de Nickel, Geosciences (2011) 50–57.
[5] T. Jaffré, M. Latham, M. Schmid, Aspects de l'influence de l'extraction du minerai de nickel sur la végétation et les sols en Nouvelle-Calédonie, Cah ORSTOM Sér Biol 12 (1977) 307–321.
[6] P. Gunkel-Grillon, C. Laporte-Magoni, M. Lemestre, N. Bazire, Toxic chromium release from nickel mining sediments in surface waters, New Caledonia, Environ. Chem. Lett. 12 (2014) 511–516.
[7] G. Losfeld, L. L'Huillier, B. Fogliani, T. Jaffré, C. Grison, Mining in New Caledonia: environmental stakes and restoration opportunities, Environ. Sci. Pollut. Res. 22 (2015) 5592–5607.
[8] S. Isnard, L. L'huillier, F. Rigault, T. Jaffré, How did the ultramafic soils shape the flora of the New Caledonian hotspot? Plant Soil 403 (2016) 53–76.
[9] Y. Pillon, J. Munzinger, H. Amir, M. Lebrun, Ultramafic soils and species sorting in the flora of New Caledonia, J. Ecol. 98 (2010) 1108–1116.
[10] R.D. Reeves, Tropical hyperaccumulators of metals and their potential for phytoextraction, Plant Soil 249 (2003) 57–65.
[11] T. Jaffré, B. Pelletier, Plantes de Nouvelle-Calédonie permettant de revégétaliser des sites miniers, SLN (NCL), Nouméa, 1992.
[12] G. Losfeld, R. Mathieu, L. L'Huillier, B. Fogliani, T. Jaffré, C. Grison, Phytoextraction from mine spoils: insights from New Caledonia, Environ. Sci. Pollut. Res. 22 (2015) 5608–5619.
[13] G. Losfeld, L. L'Huillier, B. Fogliani, S.M. Coy, C. Grison, T. Jaffré, Leaf-age and soil-plant relationships: key factors for reporting trace-elements hyperaccumulation by plants and design applications, Environ. Sci. Pollut. Res. 22 (2015) 5620–5632.
[14] C. Grison, Combining phytoextraction and ecocatalysis: a novel concept for greener chemistry, an opportunity for remediation, Environ. Sci. Pollut. Res. 22 (2015) 5589–5591.
[15] V. Escande, B.-L. Renard, C. Grison, Lewis acid catalysis and Green oxidations: sequential tandem oxidation processes induced by Mn-hyperaccumulating plants, Environ. Sci. Pollut. Res. 22 (2015) 5633–5652.
[16] V. Escande, T.K. Olszewski, C. Grison, From biodiversity to catalytic diversity: how to control the reaction mechanism by the nature of metallophytes, Environ. Sci. Pollut. Res. 22 (2015) 5653–5666.
[17] P.-A. Deyris, C. Grison, Nature, ecology and chemistry: an unusual combination for a new green catalysis, ecocatalysis, Curr. Opin. Green Sustain. Chem. 10 (2018) 6–10.
[18] C. Grison, V. Escande, Use of Certain Manganese-Accumulating Plants for Carrying Out Organic Chemistry Reactions US Patent Application 20150174566.
[19] V. Escande, A. Velati, C. Garel, B.L. Renard, E. Petit, C. Grison, Phytoextracted mining wastes for ecocatalysis: eco-Mn®, an efficient and eco-friendly plant-based catalyst for reductive amination of ketones, Green Chem. 17 (2015) 2188–2199.
[20] V. Escande, C.H. Lam, C. Grison, P.T. Anastas, EcoMnOx, a biosourced catalyst for selective aerobic oxidative cleavage of activated 1,2-diols, ACS Sustain. Chem. Eng. 5 (2017) 3214–3222.
[21] V. Escande, E. Petit, L. Garoux, C. Boulanger, C. Grison, Switchable alkene epoxidation/oxidative cleavage with H2O2/NaHCO3: efficient heterogeneous catalysis derived from biosourced eco-Mn, ACS Sustain. Chem. Eng. 3 (2015) 2704–2715.
[22] A.T.H. Lenstra, J. Dillen, The crystal structure of manganese (II) - (+/-) -1-malate trihydrate, Bull. Sociétés Chim. Belg. 92 (1983) 257–262.
[23] V. Briois, E. Fonda, S. Belin, L. Barthe, C. La Fontaine, F. Langlois, M. Ribbens, F. Villain, UVX 2010–10e Colloque sur les Sources Cohérentes et Incohérentes UV, VUV et X; Applications et Développements Récents, 2011, pp. 41–47.
[24] K. Wu, et al., Novel synthesis of Mn3(PO4)2.3H2O nanoplate as a precursor to fabricate high performance LiMnPO4/C composite for lithium-ion batteries, RSC Adv. 5 (2015) 95020–95027.
[25] M. Falk, C.H. Huang, O. Knop, Infrared studies of water in crystalline hydrates - K2fecl5.H2o (erythrosiderite) and related aquopentachloroferrates(Iii), Can. J. Chem.-Rev. Can. Chim. 53 (1979) 51–57.
[26] https://www.synchrotron-soleil.fr/fr/lignes-de-lumiere/samba, (2019).
[27] B. Ravel, M. Newville, ATHENA, ARTEMIS, HEPHAESTUS: data analysis for X-ray absorption spectroscopy using IFEFFIT, J. Synchrotron Radiat. 12 (2005) 537–541.
[28] A. Michalowicz, J. Moscovici, D. Muller-Bouvet, K. Provost, Max: Multiplatform applications for XAFS, in: *14th* Int. Conf. X-Ray Absorpt. Fine Struct. Xafs14 Proc., 2009, p. 190.
[29] A. Michalowicz, J. Moscovici, D. Muller-Bouvet, K. Provost, MAX (multiplatform applications for XAFS) new features, in: 15th Int. Conf. X-Ray Absorpt. Fine Struct. Xafs15, 2013, p. 430.
[30] Day, N. & Murray-Rust, P. COD, Crystallography open database. Available at: http://www.crystallography.net/cod/index.php. (Accessed: 01 01 2016).
[31] A. Jain, et al., Commentary: the Materials Project: a materials genome approach to accelerating materials innovation, Apl. Mater. 1 (2013).
[32] I. Bauer, H.J. Knolker, Iron Catalysis in Organic Synthesis - Chemical Reviews, ACS Publications), 2019.
[33] D.D. Diaz, P.O. Miranda, J.I. Padron, V.S. Martin, Recent Uses of Iron (III) Chloride in Organic Synthesis, 2006.
[34] W. Croft, M. Kestigian, F. Leipziger, Preparation and crystallographic properties of KMnCl3, Inorg. Chem. 4 (1965) 423–424.
[35] A.R. Kampf, S.J. Mills, F. Nestola, M.E. Ciriotti, A.V. Kasatkin, Saltonseaite, K3NaMn2+Cl6, the Mn analogue of rinneite from the salton sea, California, Am. Mineral. 98 (2013) 231–235.
[36] P.A. Deyris, E. Petit, Y.M. Legrand, S. Diliberto, C. Boulanger, V. Bert, C. Grison, Biosourced polymetallic catalysis: A surprising and efficient means to

promote the Knoevenagel condensation, Front. Chem. 6 (2018) 48, https://doi.org/10.3389/fchem.2018.00048.
[37] S. Liang, F.T.G. Bulgan, R. Zong, Y. Zhu, Effect of phase structure of MnO2 nanorod catalyst on the activity for CO oxidation, J. Phys. Chem. C 112 (2008) 5307–5315.
[38] R. Xu, X. Wang, D. Wang, K. Zhou, Y. Li, Surface structure effects in nanocrystal MnO2 and Ag/MnO2 catalytic oxidation of CO, J. Catal. 237 (2006) 426–430.
[39] S.V. Vassilev, D. Baxter, C.G. Vassileva, An overview of the behaviour of biomass during combustion: Part I Phase-mineral transformations of organic and inorganic matter, Fuel 112 (2013) 391–449.
[40] M.M. Najafpour, B. Pashaei, S. Nayeri, Calcium manganese(IV) oxides: biomimetic and efficient catalysts for water oxidation, Dalton Trans. 41 (2012) 4799–4805.
[41] A. Ramirez, P. Bogdanoff, D. Friedrich, S. Fiechter, Synthesis of Ca2Mn3O8 films and their electrochemical studies for the oxygen evolution reaction (OER) of water, Nanomater. Energy 1 (2012) 282–289.
[42] Y.J. Park, M.A. Doeff, Synthesis and electrochemical characterization of M2Mn3O8 (M=Ca, Cu) compounds and derivatives, Solid State Ionics 177 (2006) 893–900.
[43] E. Chalmin, F. Farges, G.E. Brown Jr., A pre-edge analysis of Mn K-edge XANES spectra to help determine the speciation of manganese in minerals and glasses, Contrib. Mineral. Petrol. 157 (2009) 111–126.
[44] A. Manceau, A. Gorshkov, V. Drits, Structural chemistry of Mn, Fe, Co, and Ni in manganese hydrous oxides 1Information from xanes spectroscopy, Am. Mineral. 77 (1992) 1133–1143.
[45] M. Belli, A. Scafati, A. Bianconi, S. Mobilio, L. Palladino, A. Reale, E. Burattini, X-Ray absorption near edge structures (Xanes) in simple and complex Mn compounds, Solid State Commun. 35 (1980) 355–361.
[46] M. Wilke, F. Farges, P. Petit, G. Brown, F. Martin, Oxidation state and coordination of Fe in minerals: an FeK-XANES spectroscopic study, Am. Mineral. 86 (2001) 714–730.
[47] M. Bauer, T. Kauf, J. Christoffers, H. Bertagnolli, Investigations into the metal species of the homogeneous iron(III) catalyzed Michael addition reactions, Phys. Chem. Chem. Phys. 7 (2005) 2664–2670.
[48] T. Westre, P. Kennepohl, J. DeWitt, B. Hedman, K. Hodgson, E. Solomon, A multiplet analysis of Fe K-edge 1s->3d pre-edge features of iron complexes, J. Am. Chem. Soc. 119 (1997) 6297–6314.
[49] K. Asakura, M. Nomura, H. Kuroda, Fe K-edge XANES and EXAFS of the X-ray absorption spectra of FeCl3 aqueous solutions A structural study of the solute, iron(III) chloro complexes, Bull. Chem. Soc. Jpn. 58 (1985) 1543–1550.

Further reading

[50] A. Lenstra, J. Dillen, The crystal structure of manganese (II) - (+/-) -1-malate trihydrate, Bul Soc Chim Belg 92 (1983) 257–262.